



OPEN

Bending behavior and influence parameter optimization of connection joints of disc-buckle type formwork support

Jinfeng Dong¹✉, Zelong Liao¹, Haiqing Liu¹, Zhongwei Zhao¹, Ming Lei², Zimu Chen², Liang Wang² & Xiangen Gong²

In order to systematically study the bending behavior of the connection joints of the disc-buckle type formwork support, the accurate numerical model of the disc-buckle type connection joints was obtained through the experimental on the bending behavior of the connection joints of the disc-buckle type, and the bending moment-rotation curve of the joints was verified. The analysis of the failure mode and stress distribution of the joints reveals the importance of the bending behavior of each component. By establishing an accurate numerical model of the joint, the accuracy of the bending experiment of the joint was verified, and the parametric analysis of the influence factors such as the depth of the wedge insertion the disk-plate, the initial position of the wedge insertion the disk-plate, the thickness of the wedge, material constitutive of the wedge and the thickness of the disk-plate was carried out to grasp the influence of the relevant parameters on the bending behavior of the joint. The results shown that the connection joints of the disc-buckle type formwork support were a typical semi-rigid connection joints. The thickness of the disk-plate plays a decisive role in the joint bending capacity, and the optimum thickness of the disk-plate was 10 mm. The thickness of the wedge was proportional to the joint bending capacity, and the optimal thickness of the wedge was 7 mm. The drop depth of the wedge should not exceed 6 mm during the locking process and the most suitable yield strength of the wedge was set to 450–500 MPa.

Keywords Semi-rigid connection joints, Disc-buckle type coupler high formwork support system, Bending behavior, Stress distribution, Finite element parametric analysis

With the rise of large-space and large-span building structures, the use of formwork support system is also increasing. As a type of temporary structural system, its importance has gradually been paid attention to by the building industry. At present, the research on formwork support at home and abroad mainly focuses on fastener-type and bowl buckle-type^{1–5}, and the experimental and theoretical research on the bending behavior of the connection joints and overall stability of the disc-buckle type formwork support were relatively less. In recent years, there have also been studies on the behavior of special forms of formwork supports^{6,7}. Scaffold collapse accidents occur frequently around the world. American scholars Hadipriono Fabian C. and Wang H.K analyzed 85 formwork support collapse accidents in the United States⁸, the main reasons include serious imperfections of the vertical pole, the unreasonable number and building method of the diagonal bracing, and the external impact load. The joint bending stiffness, initial imperfections and building methods have an influence on the bearing capacity of the high formwork support system^{9–13}.

As an important part of the overall structure, it is necessary to study the bending behavior of the connection joints^{14–17}. The connection joints of the formwork support can be regarded as semi-rigid connection joints, which have an influence on the overall structural stability. Chen et al.¹⁸ derived the effective length factor of the semi-rigid connection with lateral displacement on the basis of considering the semi-rigid behavior of the joints, and applied it to the calculation of the stability bearing capacity. Zhang et al.¹⁹ of Sydney found that the number of horizontal bars at the joint will affect the rotational stiffness of the joint through experimental research, and the moment-rotation curve of any joint can be fitted by a three-line model. Xiao et al.²⁰ and others think that the rotational stiffness of the joint is more appropriate at 50 kN • M/rad through the comparative analysis

¹School of Civil Engineering, Liaoning Technical University, Fuxin 123000, China. ²China Construction Fifth Engineering Division Corp., Ltd., Changsha 410004, China. ✉email: djf2252769361@163.com

of experimental and finite element, and propose that it is more accurate to consider the influence of initial geometrical imperfections. Yuan et al.²¹ and others studied the stability of fastener-type formwork support, and pointed out that the initial imperfections and the semi-rigid characteristics of the joints have a significant influence on the overall stability. Lu et al.²² and others studied the bearing capacity of fastener steel tube full hall formwork support by using the theory of stability of pressed pole with three-point rotation restraint, and the nonlinear finite element analysis considering the initial imperfections was carried out, finally, the overall instability mode was obtained. On this basis, the bearing capacity of the fastener steel tube full hall formwork support system under eccentric load was studied²³. It is very necessary to consider the initial imperfections in the finite element analysis. Zhuang et al.²⁴ set the model scaling factor according to the eigenvalue buckling analysis results to consider the influence of initial imperfections on the stability bearing capacity of high and large formwork support system. Yu et al.²⁵ and Chu et al.²⁶ integrated the lowest eigenmode with a column out-of-straightness magnitude of 1/1000 for the height of the scaffold units into the model.

Scholars from all over the world have studied the semi-rigid connection joints of the formwork support system, but only given the reference value of bending stiffness, and did not study the influencing factors of the semi-rigid connection joints in detail. In view of the particularity of the connection joints of the disc-buckle type formwork support system, the influencing factors of the bending behavior of the connection joints were complex. Master the influence of relevant parameters such as the depth of the wedge insertion the disk-plate, the initial position of the wedge insertion the disk-plate, the thickness of the wedge, the material constitutive of the wedge and the thickness of the disk-plate on the bending resistance of the joint. In this paper, the bending behavior experiments of the connection joints in the positive and negative directions were carried out, through the comparative analysis of the failure modes, the finite element parametric study of the influencing factors of the bending behavior of the connection joints was carried out. It was verified that the connection joints of the disc-buckle type were a typical semi-rigid connection joints. The influencing factors of structural stability were analyzed by experiment of the multi-parameter structural stability, and the joint bending stiffness curve was applied to the overall finite element model by establishing the nonlinear spring elements, the correctness of the finite element model was verified.

Experimental analysis on bending behavior of the connection joints of disc-buckle type formwork support

Experimental design

In this study, the structural form, experimental specimen design and experimental loading method of the disc-buckle type formwork support were the same as those of the published papers²⁹, and the stress distribution and failure mode of the joints under bending moment were mainly studied. During the loading process, it was found that the wedge was not necessarily in the middle state during the inserted into the disk-plate, so the initial position of the wedge insertion the disk-plate was also one of the factors affecting the bending behavior. The initial random position of the wedge was different after the wedge was inserted into the disk-plate. There were three conditions: the tail of the wedge was left, right and middle close to the bottom of the bolt hole of the wedge head, as shown in Fig. 1.

When analyzing the stress distribution of the joint under the bending state, seven strain gauges were arranged in this experiment. Due to the different loading directions of the joints, the positions of strain gauges 4 and 7 should be changed accordingly. The specific position of the strain measuring points were shown in Fig. 2. Strain gauge 1 and strain gauge 2 were located on the left and right sides of the hole in the bending zone on the disk-plate. Strain gauge 3 was located in the opposite position near the hole in the non-bending zone on the disk-plate. Strain gauge 1, strain gauge 2 and strain gauge 3 were located in the upper and lower directions of the disk-plate, which were used to measure the overall stress change on the disk-plate, as shown in Fig. 2A. The strain gauge 4 was located on the vertical pole in contact with the lower end of wedge head of the horizontal bar, and the change of stress on the vertical pole was measured. For the positive bending state, the position of the strain gauge 4 was located on the surface of the vertical pole in contact with the lower end of the wedge head, as shown in Fig. 2B. For the negative bending state, the position of the strain gauge 4 was located on the surface of the vertical pole in contact with the upper end of the wedge head, as shown in Fig. 2C. The h_1 in the figure indicates the distance from the center position of the strain gauge 4 to the edge of the proximal disk-plate. The strain gauges 5 and 6 were arranged at the welding position of the wedge head and the horizontal bar, which were located at the lower edge and the upper edge of the horizontal bar respectively. They were used to measure the stress change at the end of the horizontal bar. In the figure, l_1 represents the distance from the center position of the strain gauge 5

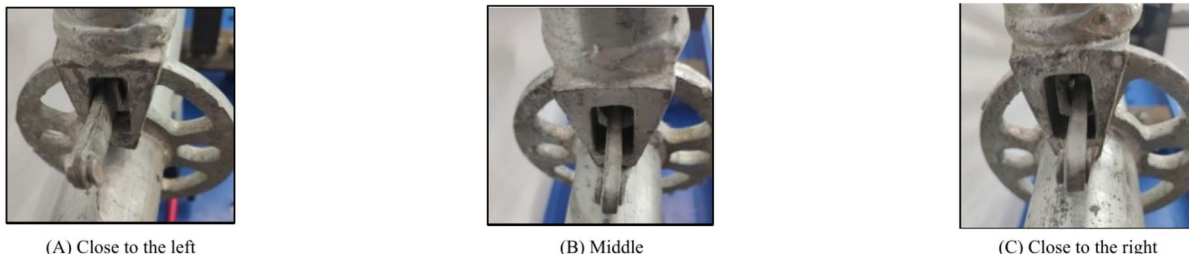


Fig. 1. Initial position of the wedge insertion the disk-plate.

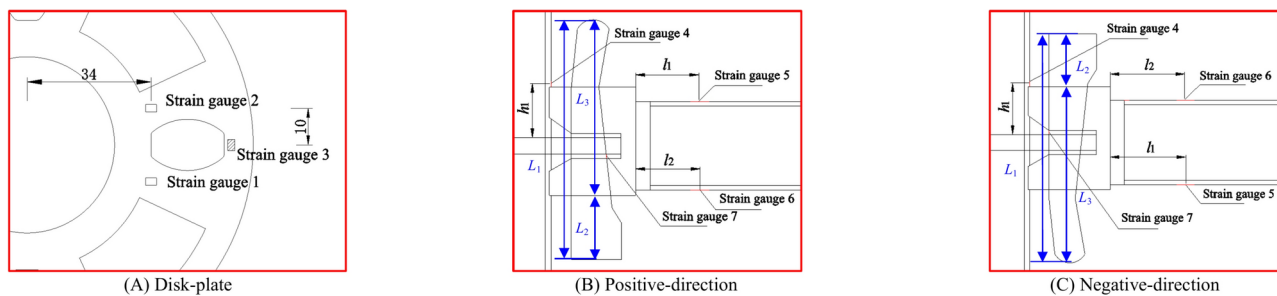


Fig. 2. Arrangement of the strain measuring point (unit: mm).

No.	L_2 (mm)	L_3 (mm)	L_1 (mm)	b (mm)	t_p (mm)	No.	L_2 (mm)	L_3 (mm)	L_1 (mm)	b (mm)	t_p (mm)
P-SJ1	30	98	128	5.80	10.02	N-SJ1	39	89	128	5.79	9.72
P-SJ2	37	91	128	6.09	9.66	N-SJ2	38	90	128	5.61	9.71
P-SJ3	39	89	128	5.60	9.80	N-SJ3	40	88	128	5.77	9.81
P-SJ4	34	94	128	6.00	9.65	N-SJ4	37	91	128	5.81	9.74
P-SJ5	39	89	128	6.00	9.79	N-SJ5	35	93	128	5.63	9.77
P-SJ6	30	98	128	5.67	9.72	N-SJ6	41	87	128	6.10	9.80
P-SJ7	28	100	128	5.95	10.00	N-SJ7	41	87	128	6.19	9.85
P-SJ8	33	95	128	5.63	9.55	N-SJ8	35	93	128	6.08	10.11

Table 1. Detailed dimensions of the insertion depth, thickness of the wedge and the disk-plate.

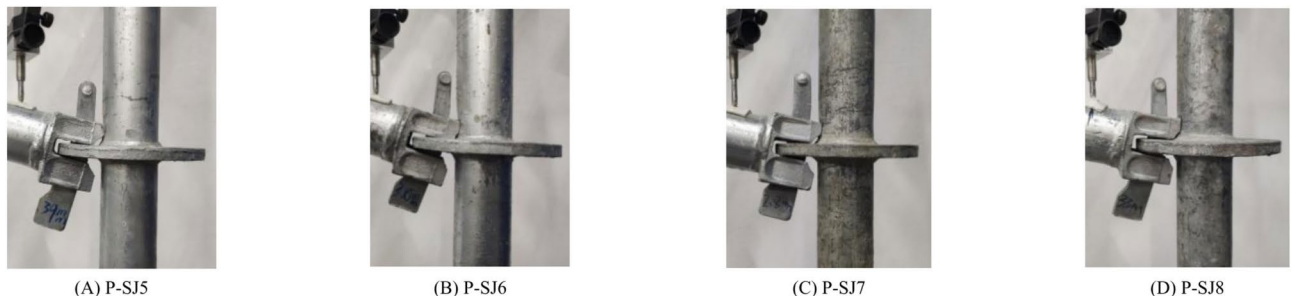


Fig. 3. Failure modes in the positive direction.

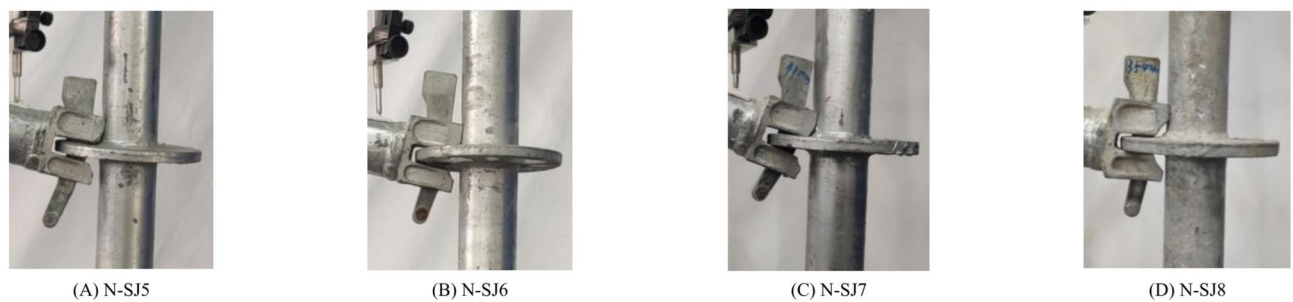
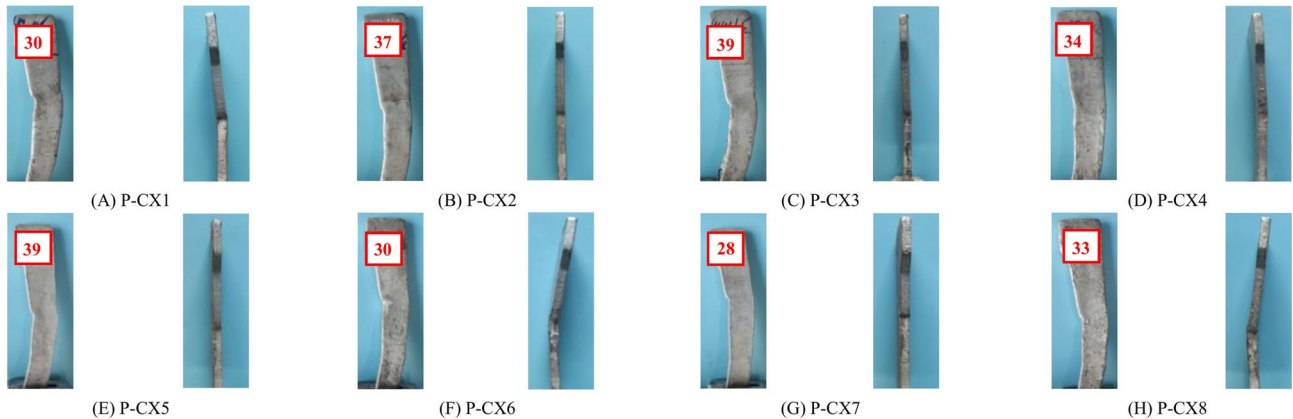
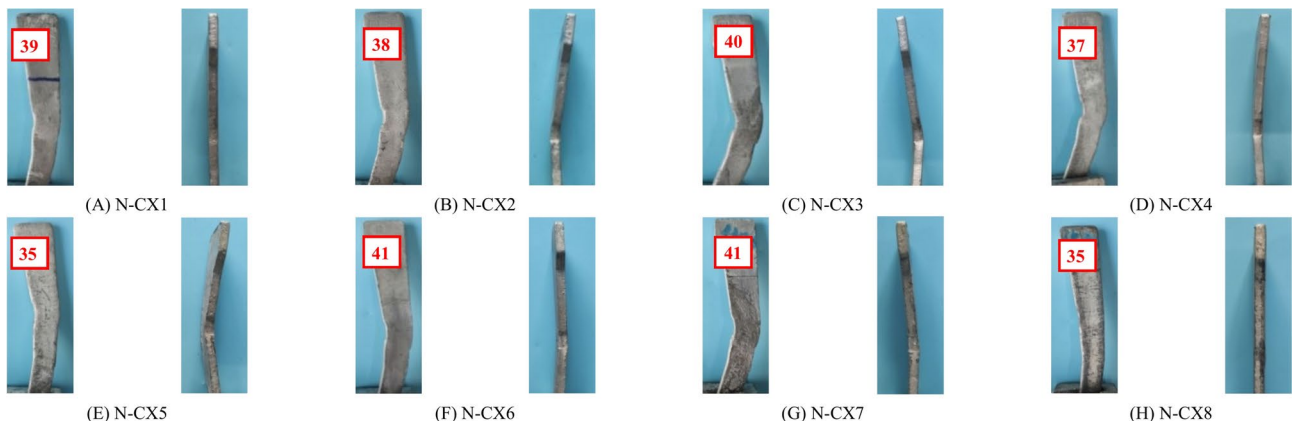
to the welding position of the wedge head and the horizontal bar, and l_2 represents the distance from the center position of the strain gauge 6 to the welding position of the the wedge head and the horizontal bar. The strain gauge 7 was arranged on the wedge, which was arranged on the side of the wedge which was prone to stress concentration at the joint with the disk-plate, to measure the stress change at the wedge. Because the strain gauges 3 and 7 were located in a special position, they were fixed by a protective coating.

Experimental results and analysis

Failure modes of the connection joints

The design parameters of the bending behavior experiment of 8 groups of joint of positive and negative were shown in Table 1. In order to describe the depth of the wedge insertion the disk-plate, three variables were introduced, as shown in the blue of Fig. 2, that was, the total length of the wedge was set to L_1 . For the standard specimen, L_1 was set to 128 mm, L_2 represents the length of the wedge exposed outside the wedge head after it was inserted into the disk-plate and self-locking, and L_3 was the remaining length of the wedge. Therefore, the depth of the wedge insertion the disk-plate can be compared with the value of L_2 , the thickness of the wedge was represented by “ b ”, and the thickness of the disk-plate was represented by “ t_p ”.

The failure modes of the connection joints of the disc-buckle type formwork support in the positive-direction and in the negative-direction bending state were shown in Figs. 3 and 4. At the initial stage of loading, the specimen had no obvious deformation, the joint bending stiffness was larger when the bending state was small. The joint bending stiffness decreases with the increase of bending state. When the bending moment reaches a peak, the displacement increases sharply when the bending moment increases little. At this time, the buckling failure occurs at the joint, and the fracture failure does not appear in the wedge and its components. At this

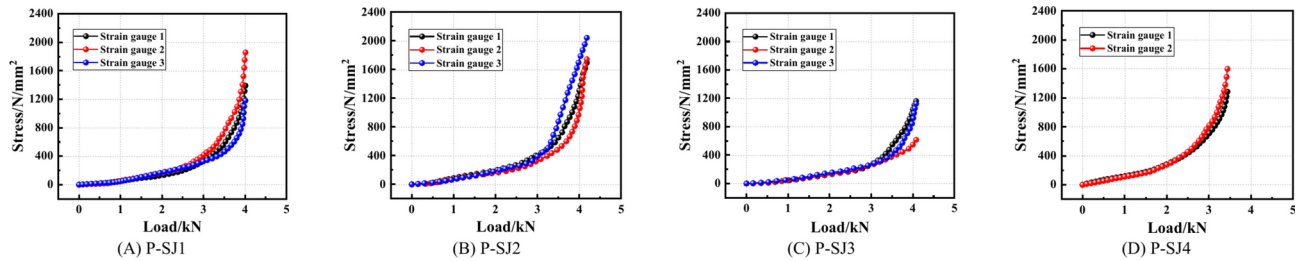
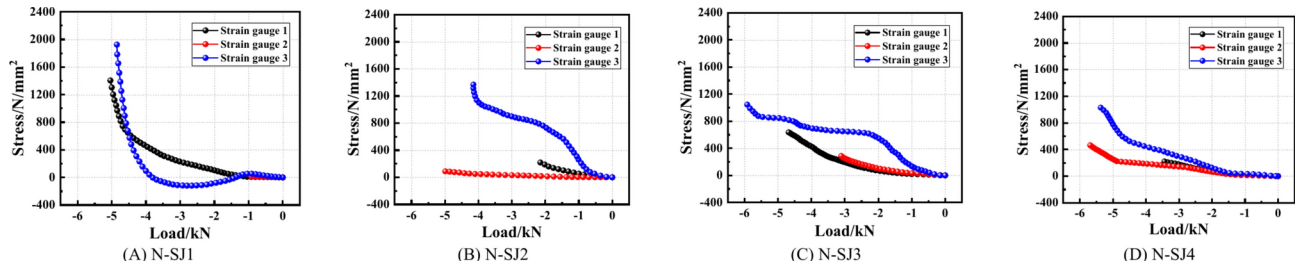
**Fig. 4.** Failure modes in the negative direction.**Fig. 5.** Wedge failure modes in the positive direction (unit: mm).**Fig. 6.** Wedge failure modes in the negative directive (unit: mm).

time, it was observed that the contact part between the upper part of the wedge and the vertical pole had been separated, and the horizontal bar had a large rotation angle relative to the vertical pole. It can be approximately considered that the joint reaches the bending limit state.

The preliminary analysis shown that the failure mode was mainly affected by two factors when the connection joints were in the bending state. Firstly, the initial state of each component mainly includes the depth of the wedge insertion the disk-plate and initial position of the wedge insertion the disk-plate. Secondly, the material properties of each component mainly include the thickness of the wedge, the material constitutive of the wedge, the thickness of the disk-plate and the buckling behavior of the vertical pole. The buckling behavior of the vertical pole was random and cannot be quantitatively analyzed.

The failure modes of the wedge in the bending state were shown in Figs. 5 and 6. The number in the box represents the L_2 value, and unit is mm. When the joint was in a positive bending state, the failure mode of the

No	L_2 (mm)	h_1 (mm)	l_1 (mm)	l_2 (mm)
P-SJ1	30	21	10	7
P-SJ2	37	22	14	13
P-SJ3	39	21	15	13
P-SJ4	34	18	15	14
N-SJ1	39	33	20	20
N-SJ2	38	35	15	24
N-SJ3	40	37	23	25
N-SJ4	37	24	22	17

Table 2. Detailed position dimensions of strain gauge measuring point.**Fig. 7.** Stress–load curves of the disk-plate strain measuring point in the positive direction.**Fig. 8.** Stress–load curves of the disk-plate strain measuring point in the negative direction.

wedge was serious when the depth of the wedge insertion the disk-plate was relatively large. As shown that the damage degree of the failure modes of the wedge were more serious in the negative direction, indicated that when the joint was in the negative bending state, the material properties requirements of the wedge were higher.

Stress distribution

During the positive and negative bending experiments, the stress changes at the joints of P-SJ1~P-SJ4 and N-SJ1~N-SJ4 specimens were measured respectively. The position and size of the measuring points of the strain gauges in each group were shown in Table 2.

(1) Stress distribution of disk-plate.

For the positive bending state, the stress–load curves of the three strain gauge measuring points at the disk-plate position were shown in Fig. 7. For the experiment of the P-SJ4, the strain gauge 3 was failed, and the other groups of experimental strain gauges in the positive experiments were effective. From Fig. 7, it can be seen that at the initial stage of loading, with the increase of load, the stress of the three positions on the disk-plate was almost the same. As the load continues to increase, the stress of the three strain measuring points at the disk-plate position will be different, but the overall difference was not large. The stress distribution was very uniform, indicated that the stress difference between the tensile zone of the bending surface and the tensile zone of the non-bending surface was not significant when the joint was in the positive bending state.

For the negative bending state, the stress–load curves of the three strain gauge measuring points at the disk-plate position were shown in Fig. 8. For the experiment of the N-SJ1, the strain gauge 2 was failed, for the experiment of the N-SJ2, the strain gauge 1 was basically failed. In the experiment of the N-SJ3, the strain gauges 1 and 2 were failed when the joint was about to buckle. The experiment of the N-SJ4, the strain gauge 1 was basically failed. It can be seen that when the joint was in a negative bending state, the stress distribution on the

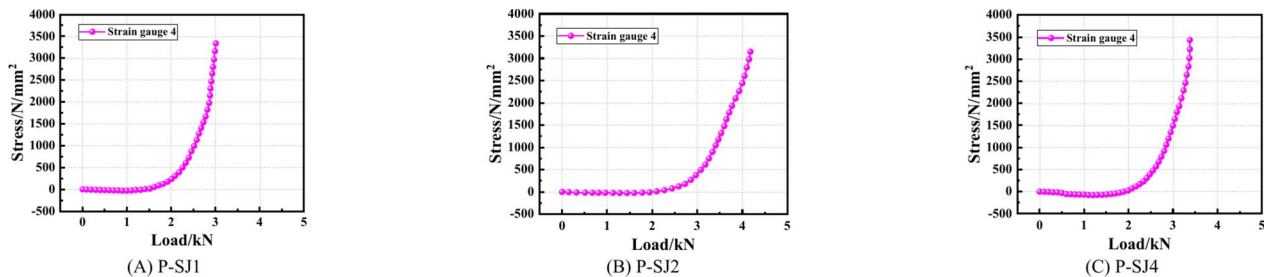


Fig. 9. Stress–load curves of the vertical pole strain measuring point in the positive direction.

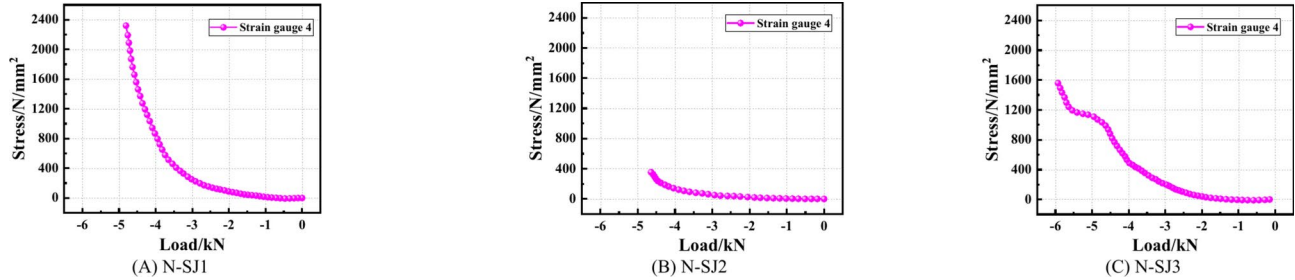


Fig. 10. Stress–load curves of the vertical pole strain measuring point in the negative direction.

disk-plate was affected, and the impact was greater. It can be seen from Fig. 8 that at the initial stage of loading, with the increase of load, the stress at the three positions on the disk-plate has a gap, and the stress value at the strain measuring point 3 was too large. With the continuous increase of load, the stress at the strain measuring point 3 was obviously faster than the stress at the strain measuring point 1 and 2, indicated that the stress in the tensile zone of the bending surface was not as large as that in the tensile zone of the non-bending surface. When the joint was in a negative bending state, the material properties requirements of the disk-plate for the insertion position of the wedge were higher.

By comparing the above results, it can be found that the stress state on the disk-plate shows a relatively uniform development trend when the joint was in the positive bending state and the overall stress shown a higher level. The stress state on the disk-plate shows an uneven development trend when the joint was in the negative bending state. The stress in the tension zone of the bending surface shown a lower level, but the stress in the tension zone of the non-bending surface shown a higher level, indicated that for the positive bending state, the force capacity of the disk-plate was generally put forward higher requirements. For the negative bending state, higher requirements were put forward for the force capacity of the wedge insertion position on the disk-plate.

(2) Stress distribution of vertical pole buckling position.

For the positive bending state, the stress-load curves of the strain gauge measuring point at the buckling position of the vertical pole were shown in Fig. 9. The strain gauges of the corresponding measuring points in the experiment of the P-SJ3 was failed, and the other groups of experimental data were complete. As can be seen from Fig. 9, at the beginning of loading, with the increase of load, the buckling position of the vertical pole shown a small amplitude of compression. As the load continues to increase, the buckling position on the vertical pole was in a tensile state, and the growth rate was very fast. Finally, when the joint reaches the ultimate state of bending capacity, the stress on the vertical pole also reaches a higher level, which was higher than the tensile stress value on the disk-plate.

For the negative bending state, the stress-load curves of the strain gauge measuring point at the buckling position of the vertical pole were shown in Fig. 10. The strain gauges of the corresponding measuring points in the experiment of the N-SJ2 was failed in the later stage. the strain gauges of the corresponding measuring points in the experiment of the N-SJ4 was failed, and the other groups of experimental data were complete. As can be seen from Fig. 10, in the initial stage of loading, with the increase of load, the buckling position on the vertical pole shown a small degree of compression. As the load continues to increase, the buckling position on the vertical pole shown a tensile state, and the growth rate was very fast. Finally, when the joint reaches the ultimate state of bending capacity, the stress on the vertical pole also reaches a higher level, which was not much different from the tensile stress value on the disk-plate. Compared with the positive stress state, it was found that when the joint was in the negative bending state, the stress values of the buckling position on the vertical pole were only 2/3 of the former, which indicated that the buckling behavior of the vertical pole was higher when the joint was in the positive bending state.

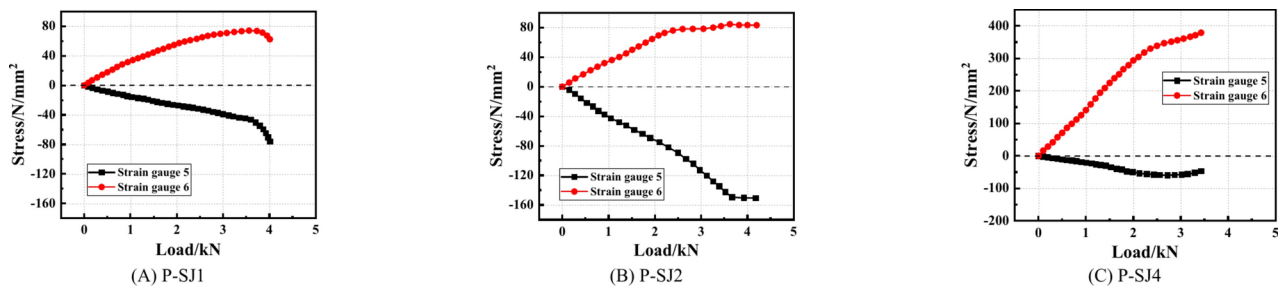


Fig. 11. Stress–load curves of the horizontal bar strain measuring point in the positive direction.

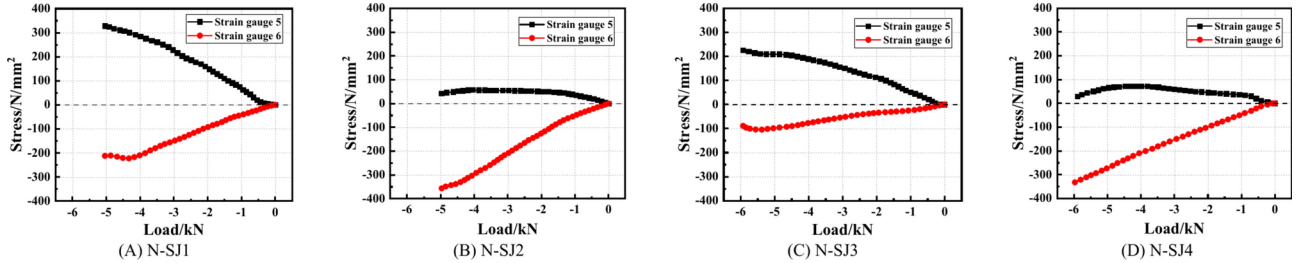


Fig. 12. Stress–load curves of the horizontal bar strain measuring point in the negative direction.

(3) Stress distribution of horizontal bar buckling position.

For the positive bending state, the stress–load curves of the strain gauge measuring point at the buckling position of the horizontal bar were shown in Fig. 11. The strain gauges of the corresponding measuring points in the experiment of the P-SJ3 was failed, and the other groups of experimental data were complete. For the position of the strain gauge measuring point on the horizontal bar of the experiment of the P-SJ1, the distance from the joint of the experiments of the P-SJ2 and P-SJ4 were relatively close, as shown in Fig. 11. It can be seen that the tensile and compressive stress values on the horizontal bar of the experiment of the P-SJ1 was relatively close, and the tensile and compressive stress values on the horizontal bar of the experiments of the P-SJ2 and P-SJ4 were quite different, indicated that the position farther from the joint was more likely to have the difference between tension and compression, and this change was not regular.

For the negative bending state, the stress–load curves of the strain gauge measuring point at the buckling position of the horizontal bar were shown in Fig. 12. For all the negative experimental horizontal bars, the distance between the position of the strain gauge measuring point and the joint was not much different. As can be seen in Fig. 12, the distance between the tensile and compressive stress measuring points on the experiments of the N-SJ1 and N-SJ3 horizontal bars were not much different. The distance between the tensile and compressive stress measuring points on the experiments of the N-SJ2 and N-SJ4 horizontal bars were quite different. When the joint was in a negative bending state, the symmetry of the stress value of the tensile and compressive state on the horizontal bar was related to the symmetry of the distance from the joint, and had nothing to do with the distance from the joint.

FEA of bending behavior

Constitutive model of material

Before establishing the finite element model of joint bending experimental specimen, the constitutive model of each component material was determined, included horizontal bar, vertical pole, wedge and wedge head. Tensile testing of steel pipes was designed according to the relevant requirements of GB/T228.1-2010 “Metalllic materials Tensile testing, Part 1: Method of test at room temperature”²⁸. Horizontal bars and vertical poles can be made into standard arc specimens according to the specification because of their structural modeling standards, as shown in Fig. 13A. The structure of the wedge was irregular, so the relative standard specimen was made according to its size, as shown in Fig. 13B.

The material tensile testing was carried out by universal testing machine²⁷. The axial tension was collected by the universal testing machine, and the displacement variation was collected by extensometer connected with the testing machine. The stress–strain curves of each component were obtained by testings as shown in Fig. 14.

Establishment of finite element model

The constitutive model used in the finite element numerical analysis was obtained by simplifying the real data of the constitutive experiment. The experimental data of SG-SJ-1 was used for the constitutive model of the horizontal bar, the experimental data of LG-SJ-1 was used for the constitutive model of the vertical pole, the

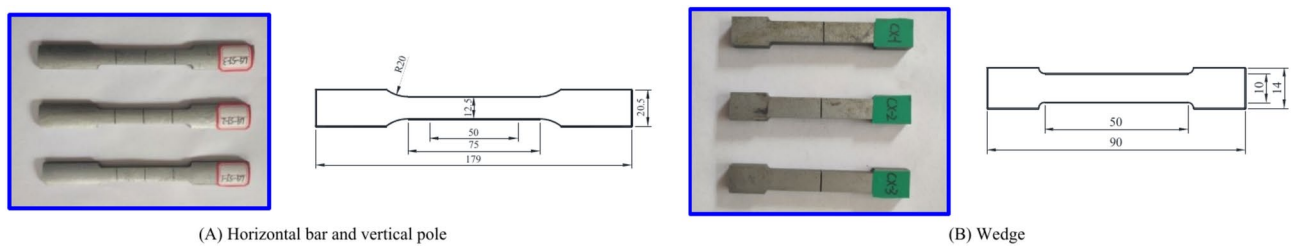


Fig. 13. Dimensions of tensile testing specimens (unit: mm).

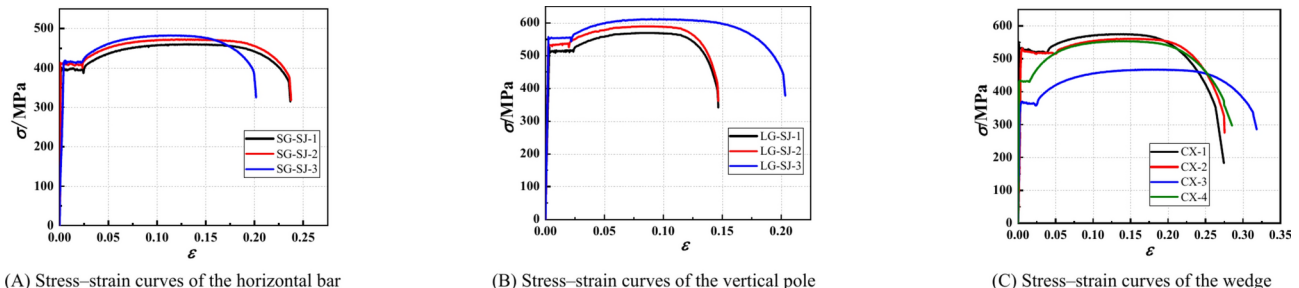


Fig. 14. Constitutive model of each component.

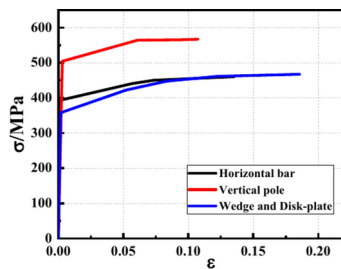


Fig. 15. Constitutive model of materials.

experimental data of CX-3 was used for the constitutive model of the wedge and the disk-plate, the constitutive models of the three materials were shown in Fig. 15.

The outer diameter and wall thickness of the horizontal bar were set to 48 mm and 2.5 mm, respectively, the outer diameter and wall thickness of the vertical pole were set to 48 mm and 3.2 mm, respectively. According to the results of material tensile testing, the elastic modulus of the horizontal bar and the vertical pole material was set to 2.06×10^5 N/mm², the elastic modulus of the wedge and the disk-plate material were set to 1.95×10^5 N/mm², the Poisson's ratio was set to 0.3, the empirical value of the friction coefficient was set to 0.2, and the normal stiffness was set to 1.0.

ANSYS finite element analysis software was used to establish the refined finite element model of the connection joints. As shown in Fig. 16, the solid185 element was discretized into a geometrical model, and contact elements CONTA174 and TARGE170 were used to simulate the mechanical behavior of the wedge and the disk-plate respectively. The solid was divided into a unified mesh size, using a mesh size of 0.004 m, and then the vertical pole, wedge and disk-plate were meshed to speed up the convergence speed. After the mesh was divided, the mesh density of the surface should be encrypted, mainly the side of the vertical pole, the outer surface of the wedge and the upper and lower surfaces of the disk-plate, and the contact line between the disk-plate and the wedge should be encrypted. The four contact pairs were established to greatly accelerate the convergence speed, they were respectively wedge and the side wall of the hole on upper and lower of the wedge head at the end of the horizontal bar, the side of the wedge and the side wall of the disk-plate hole, the wedge and the hole position of the disk-plate and the wedge at the end of the horizontal bar and the side wall of the vertical pole.

The boundary conditions of the finite element model were set up according to the experimental conditions (Fig. 17), and the upper and lower ends of the vertical pole were fixed by limiting the translational degrees of freedom in the X, Y and Z directions. A rigid surface was established in the middle of the end of the horizontal bar through a rigid element CERIG, which connected the loading point with each node at the end of the horizontal bar, the displacement constraint at the end of the horizontal bar was directly applied to the loading

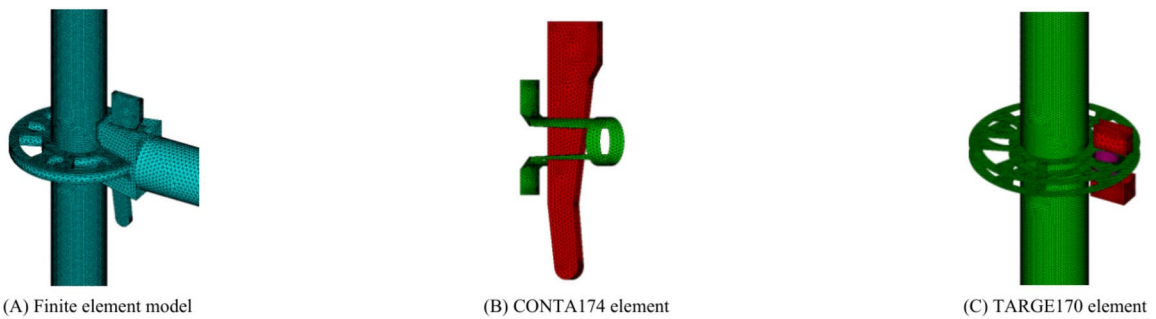


Fig. 16. Fine numerical model of the connection joints.

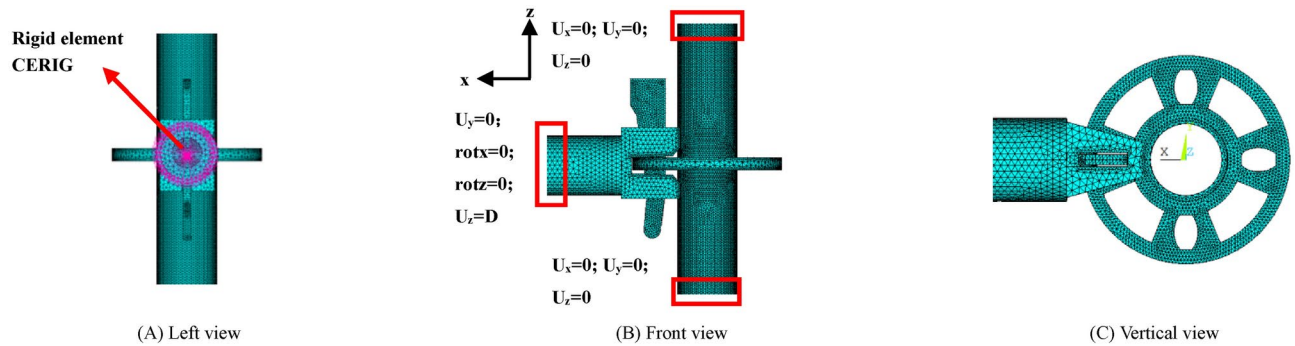


Fig. 17. Boundary conditions of the finite element model.

point, the translational degree of freedom in the Y direction of the end of the horizontal bar was fixed, and the displacement D in the Z direction was applied to the loading point at the end of the horizontal bar to apply the bending moment.

Comparative analysis of bending behavior

As knew that the bending stiffness and bending capacity were closely related to the initial manufacturing error through the analysis of the experimental data, so it was very necessary to carry out parametric analysis through finite element analysis. By comparing the finite element numerical simulation results with the experimental results, the accurate numerical model of the disc-buckle type connection joints was verified.

The simulation results of the finite element model were compared with the experimental results²⁹ (Fig. 18). From the comparison diagram, we found that the finite element model can accurately predict the positive bending stiffness and bending capacity, and the finite element model can effectively predict the negative bending capacity, but the prediction of the negative bending stiffness was not very accurate, which may be related to the initial position of the wedge insertion the disk-plate and the buckling behavior of the vertical pole, and it was also possible that the influence of geometric imperfection was not considered.

Through the above conclusions, the reliability of the finite element model to predict the bending capacity of the connection joints of the disc-buckle type formwork support was verified. The initial stiffness, pre-yield stiffness change and yield bending capacity of the forward finite element analysis were very accurate, and the error was basically within the range. The ability to predict the post-yield stiffness change and bending capacity was deviated, but the ability of the finite element to predict the bending capacity was high, basically about 20% higher. the initial stiffness and stiffness change trend of the negative finite element analysis were relatively poor, which were basically greater than the experimental value, but predict negative bending capacity was very strong.

The comparison of the failure modes between the experimental and the finite element analysis were shown in Fig. 19. The results shown that the finite element model can accurately predict the failure mode of the connection joints of the disc-buckle formwork support.

Analysis on influence parameters of bending behavior

Through the failure mode analysis in “Failure modes of the connection joints” section, it can be known that the bending behavior of the connection joints was related to the depth of the wedge insertion the disk-plate, the initial position of the wedge insertion the disk-plate, the thickness of the wedge and the disk-plate, the material constitutive of the wedge and the buckling behavior of the vertical pole, the buckling behavior analysis of the vertical pole cannot be quantitatively analyzed, which was an uncertainty factor. The following parametric analysis was carried out on the influencing factors.

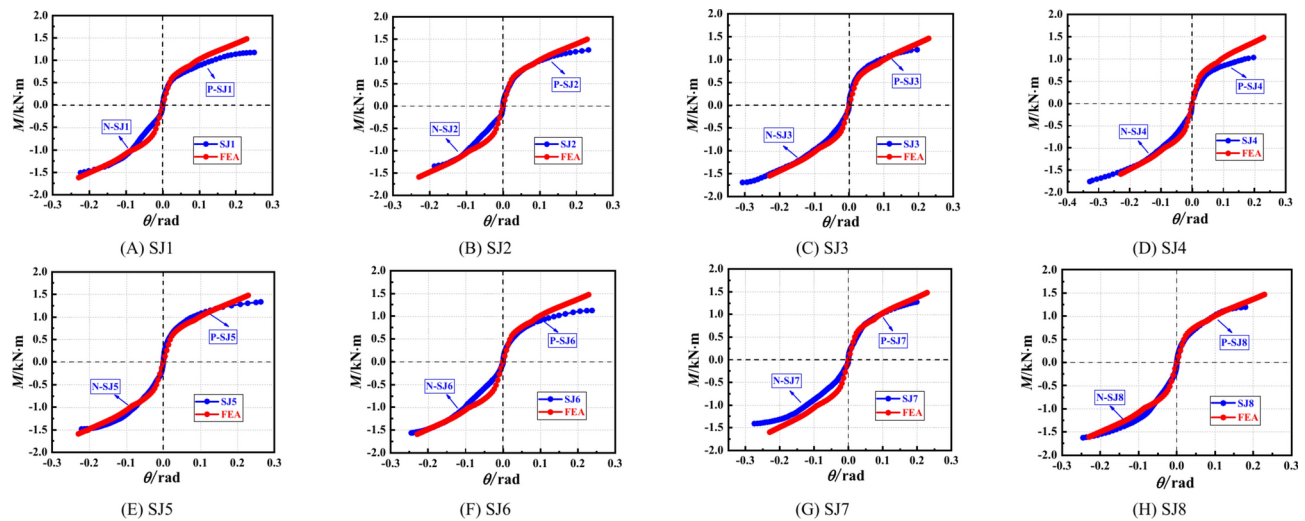


Fig. 18. Comparative analysis of experimental and finite element results.

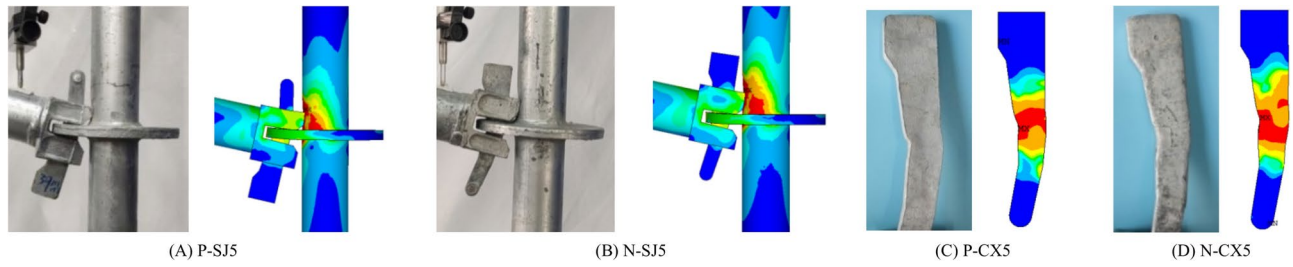


Fig. 19. Finite element comparative analysis of failure modes.

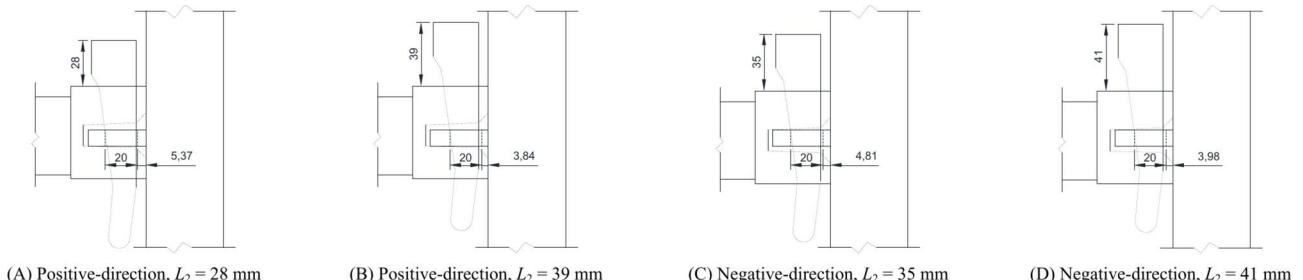


Fig. 20. Location diagram of the wedge insertion the disk-plate.

Depth of the wedge insertion the disk-plate

There were generally two reasons for the different depth of the wedge insertion the disk-plate. The first one was caused by the manufacturing error of the component, the second was caused by the mutual embedding of the wedge and the bolt hole on the disk-plate. For the first condition, it was realized by controlling the position of the bolt hole on the disk-plate (Fig. 20), and the wedge and the side wall of the bolt hole were not embedded. According to the experimental results, when the joint was in the positive bending state, $L_2 = 28 \sim 42$ mm, when the joint was in the negative bending state, $L_2 = 35 \sim 42$ mm. The thickness of the wedge was set to 5.67 mm, the thickness of the disk-plate was set to 10 mm, and the initial position of the wedge was in the middle.

Figure 21 showed that the different insertion depth of the wedge caused by manufacturing error had little influence on the bending capacity of the connection joints. For the bending state in the positive direction, the insertion depth had little influence on the bending capacity, for the bending state in the negation direction, the insertion depth had an influence on the bending capacity, but there was no regularity, which indicated that the manufacturing error had little influence on the bending capacity of the connection joints.



Fig. 21. Influence of the wedge insertion depth on joint bending capacity.

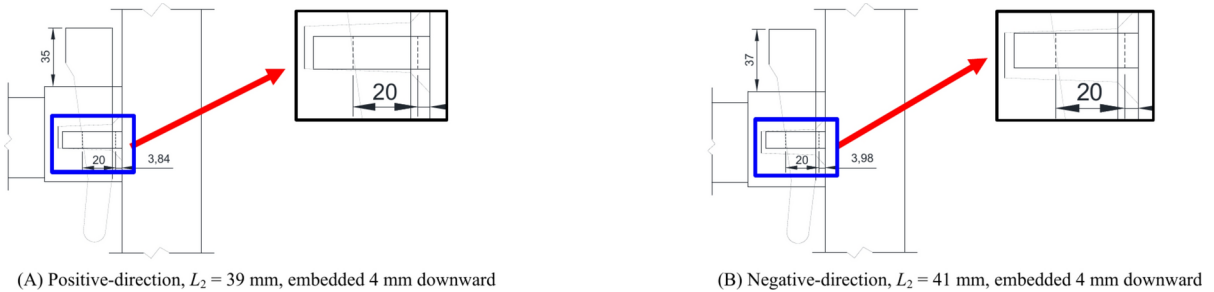


Fig. 22. Location diagram of the wedge insertion the disk-plate.

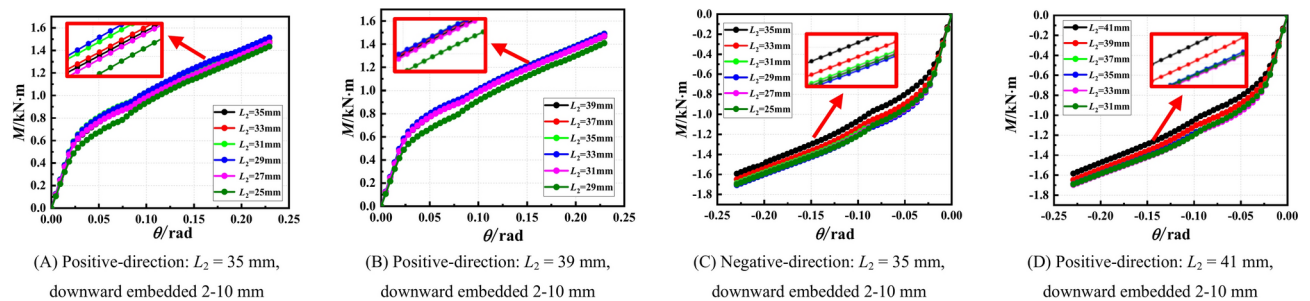


Fig. 23. Influence of the wedge insertion depth on joint bending capacity.

For the second condition, it was caused by the mutual embedding of the wedge and the bolt hole on the disk-plate (Fig. 22), which was studied by controlling the insertion depth of the wedge, the wedge was embedded in the side wall of the bolt hole, and there was no difference in the bolt hole position on the disk-plate. When the joint was in the positive bending state, the variation of the bending capacity of the downward embedding process was studied when $L_2 = 35$ mm and 39 mm. When the joint was in the negative bending state, and $L_2 = 35$ mm and 41 mm was studied.

As showed in Fig. 23, the bending capacity would not change significantly with the increase of the embedded depth in the positive bending state, when the embedded depth was greater than 6 mm, the bending capacity would decrease. The bending capacity increase with the increase of the embedded depth in the negative bending state, however, when the embedded depth was greater than 6 mm, the bending capacity would not increase. Embedded depth had no influence on the positive bending capacity, but the appropriate embedded depth can improve the negative bending capacity.

In summary, The different insertion depth caused by manufacturing errors had no influence on the bending capacity of the connection joints, and different embedded depth had no influence on the bending capacity in the positive direction, and the greater the depth was, the smaller the bending capacity will be. Appropriate embedded depth had an improve influence on the bending capacity in the negative direction. The insertion depth caused by manufacturing error had no influence on the initial bending stiffness, but the different insertion depth caused by mutual embedding had influence on the initial bending stiffness. The deeper the embedding was, the smaller the initial bending stiffness in the positive direction, and the larger the initial bending stiffness in the negative direction. Therefore, in the actual construction, as long as the wedge was connected to form a self-locking, the embedded depth of the wedge in the self-locking process should not be greater than 6 mm.

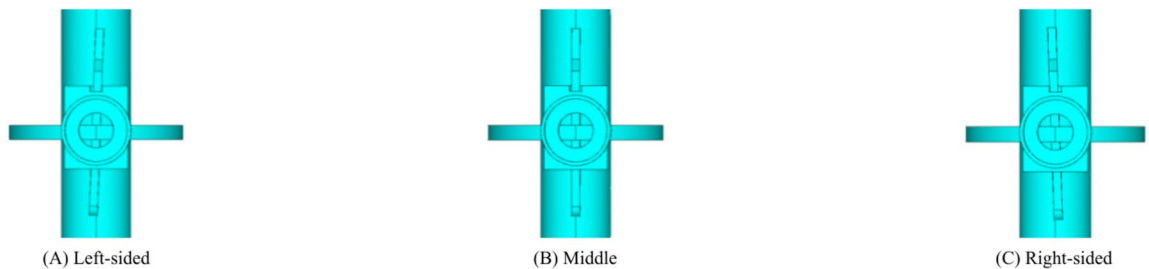


Fig. 24. Initial position condition of the wedge.

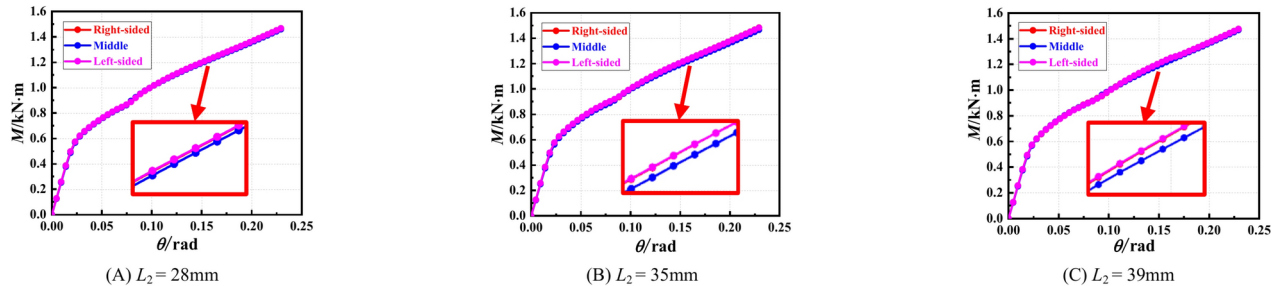


Fig. 25. Influence analysis of the initial position of the wedge in the positive bending.

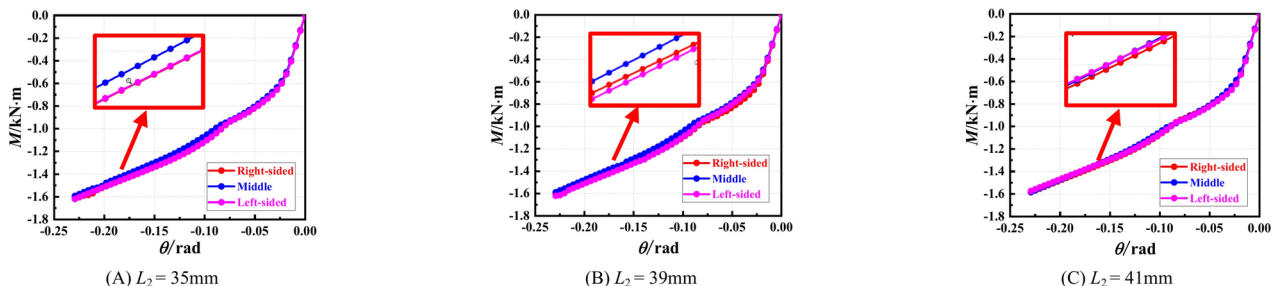


Fig. 26. Influence analysis of the initial position of the wedge in the negative bending.

Initial position of the wedge insertion the disk-plate

The initial position of the wedge insertion the disk-plate was shown in Fig. 24. Three conditions were mainly considered, which were left-sided, middle and right-sided. The influence of the location of $L_2 = 28$ mm, 35 mm and 39 mm was considered when the joint was in the positive bending state. The influence of the location of $L_2 = 35$ mm, 39 mm and 41 mm was considered when the joint was in the negative bending state. The thickness of the wedge was set to 6 mm, the thickness of the disk-plate was set to 10 mm, and the initial position of the wedge was in the middle.

No matter whether the joint was in the positive or the negative bending state, the initial position of the wedge had little influence on the bending capacity and initial bending stiffness of the connection joints. When the joint was in the positive bending state (Fig. 25), the deviation of the initial position can improve the bending capacity for the condition of smaller insertion depth.

When the joint was in the negative bending (Fig. 26), the greater the insertion depth was, the more obvious the improvement effect of the joint bending capacity was. In a word, the initial position deviation would not reduce the joint bending capacity, but also slightly improved.

Thickness of the wedge

When the joint was in the positive bending state, the influence of the thickness of the wedge was considered when L_2 was set to 28 mm and 39 mm, the thickness of the disk-plate was set to 7 mm and 10 mm. The thickness of the wedge was set to 4 mm, 5 mm, 6 mm, 7 mm, 8 mm, and the initial position of the wedge was in the middle. When the joint was in the negative bending state, the influence of the thickness of the wedge was considered when L_2 was set to 35 mm and 41 mm, other conditions were the same as when the joint was in the positive bending state. With the increase of the thickness of the wedge, the joint moment-rotation curves were shown in Fig. 27. No matter the joint was in the positive and the negative bending state, the joint initial stiffness and

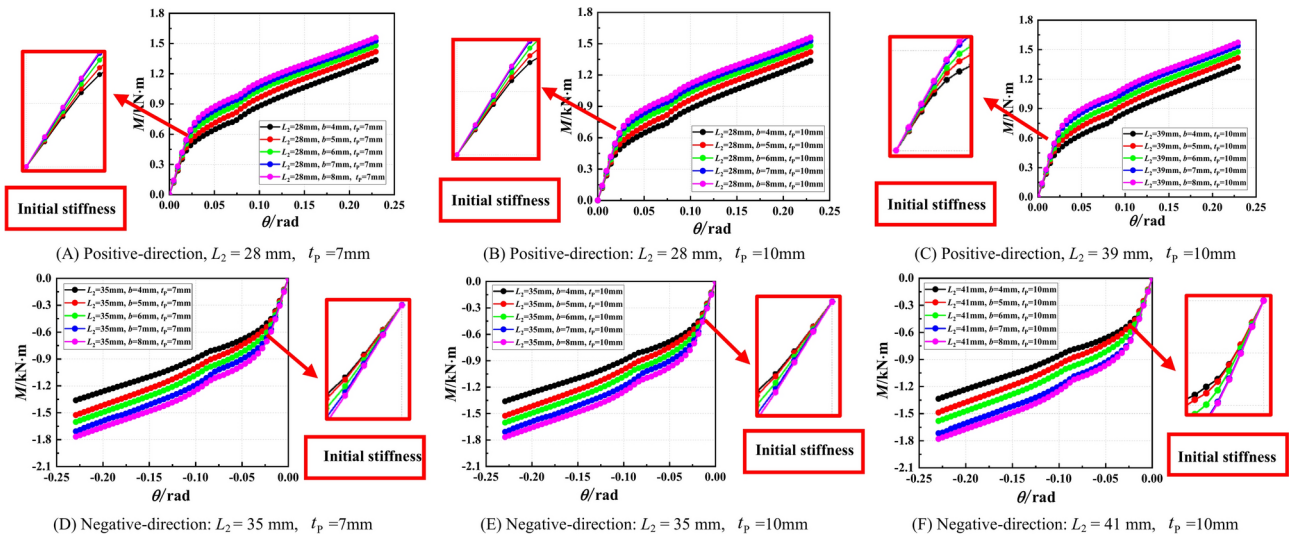


Fig. 27. Influence of the thickness of the wedge on bending capacity.

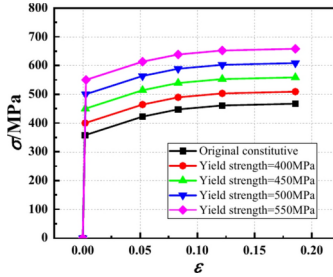


Fig. 28. Material constitutive condition of the wedge.

bending capacity were increased with the increase of the thickness of the wedge, when the thickness of the wedge exceed 7 mm, the bending capacity of the joint was also improved, but the improvement effect was not obvious. Based on the economy and portability, the optimal thickness of the wedge was determined to be 7 mm.

Material constitutive of the wedge

The constitutive of the material was considered when the thickness of the disk-plate was set to 7 mm and 10 mm and the thickness of the wedge was set to 5 mm and 8 mm. The material constitutive of the wedge was shown in Fig. 28, and the initial position of the wedge was in the middle. When the joint was in the positive bending, L_2 was set to 28 mm, when the joint was in the negative bending, L_2 was set to 35 mm.

With the change of material constitutive model of wedge, the joint bending moment-rotation curves of positive and negative bending were shown in Fig. 29. As seen from Fig. 29 that, the joint bending capacity increased with the increase of the material constitutive of the wedge, and the optimum yield strength was between 450 and 500 MPa. The greater the thickness of the disk-plate, the more obvious the increase of the joint bending capacity with the increase of the material constitutive of the wedge, especially the post bending capacity. With the increase of the thickness of the wedge, the influence of the material constitutive on the joint bending capacity was not very obvious.

The increase in the material constitutive of the wedge had little effect on the joint initial bending stiffness, and the joint initial bending stiffness did not increase with the increase in the material constitutive of the wedge. The above analysis was also applicable for positive and negative bending joints.

Thickness of the disk-plate

When the joint was in the positive bending state, the influence of the thickness of the disk-plate was considered when L_2 was set to 28 mm and 39 mm, the thickness of the wedge was set to 5.67 mm and 7 mm. The thickness of the disk-plate was set to 7 mm, 8 mm, 9 mm, 10 mm, 11 mm and 11.5 mm, and the initial position of the wedge was in the middle. With the increase of the thickness of the disk-plate, the variation of the bending moment-rotation curves were shown in Fig. 30. When the joint was in the negative bending state, the influence of the thickness of the disk-plate was considered when L_2 was set to 35 mm and 41 mm.

Above analysis, it can be seen that regardless of the joint was in the positive and negative bending state, the thickness of the disk-plate had little effect on the joint initial stiffness and had a significant effect on the joint

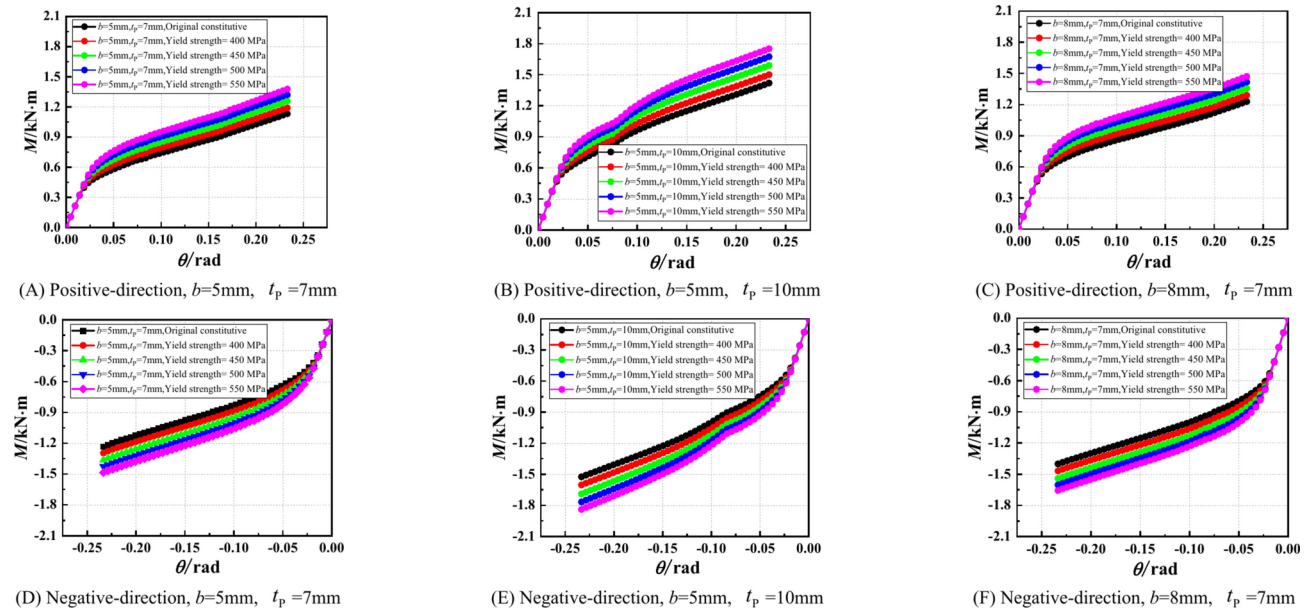


Fig. 29. Influence of the material constitutive of the wedge on joint bending capacity.

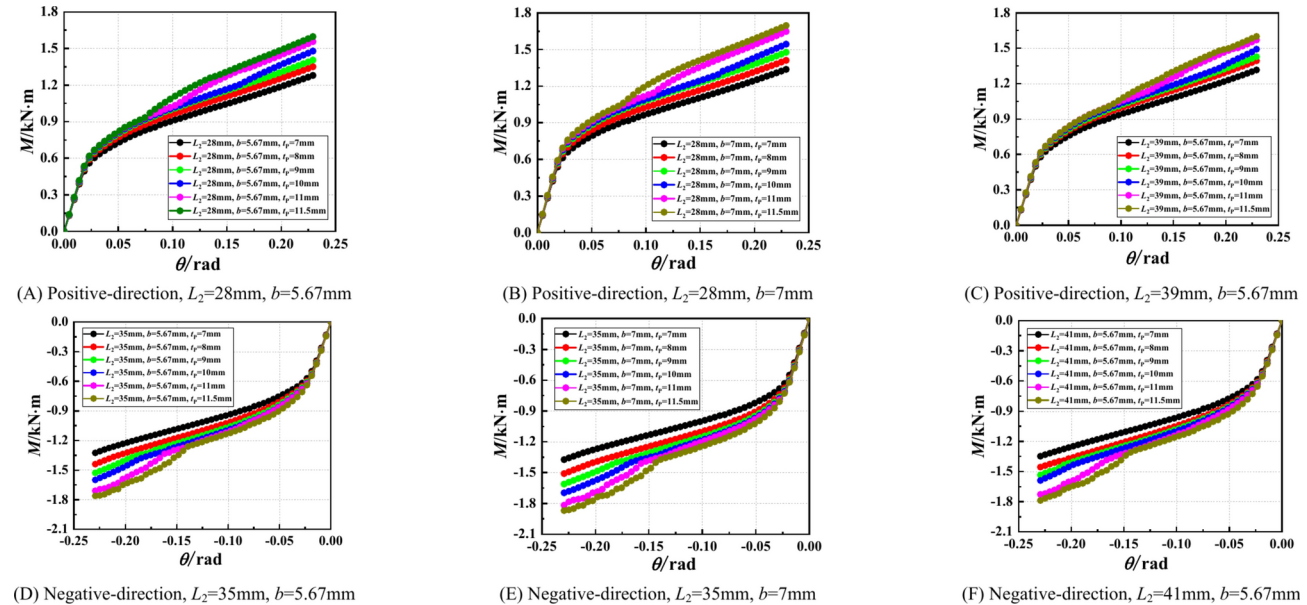


Fig. 30. Influence of the thickness of the disk-plate on joint bending capacity.

bending capacity, with the increase of the thickness of the disk-plate, the bending capacity of the joint was gradually improved, especially after the thickness of the disk-plate was greater than 10 mm, the joint bending capacity was more obvious, however, considering the economy and portability, it was not necessary to choose the maximum thickness of the disk-plate, so the optimum thickness of the disk-plate was 10 mm. By comparing Fig. 30A,B,D,E, it can be seen that the greater the thickness of the wedge, the more obvious the effect of the thickness of the disk-plate on the joint bending capacity. However, it can be seen from Fig. 27 that the greater the thickness of the disk-plate, the more obvious the effect of the thickness of the wedge on the joint bending capacity, indicated that the thickness of the disk-plate had a decisive effect on the joint bending capacity.

No.	Condition	Lift height (m)	Experimental value		Finite element value		Error (%)
			Stability bearing capacity (kN)	Increase percentage (%)	Stability bearing capacity (kN)	Increase percentage (%)	
1	Central pole	1.5	141.20	0	143.42	0	1.57
2	Central pole	0.5 + 1.0	189.28	34	189.30	32	0.01
3	Side pole	0.5 + 1.0	188.73	0	177.95	0	-5.71
4	Side pole	0.5 + 0.5 + 0.5	210.87	12	213.36	20	1.18
5	Corner pole	0.5 + 1.0	170.02	0	177.21	0	4.23
6	Corner pole	0.5 + 0.5 + 0.5	199.86	18	201.81	14	0.98

Table 3. The results of the comparison analysis between the experimental and the finite element.

Experimental analysis on structural stability of the disc-buckle type formwork support

Experimental design

The experimental model was selected based on the minimum unit in the high formwork support system, and the experimental design was carried out by considering the three working conditions in the high formwork support system, namely, working conditions of the central pole, side pole and corner pole. The stability bearing capacity of multi-working condition minimum unit vertical pole was studied and compared with the finite element results to verify the accuracy of the experimental model. Subsequently, the factors affecting the stability of high formwork support system were analyzed. According to the conclusion of parametric analysis, it was more persuasive.

Experimental specimens include 1.2 m and 0.9 m horizontal bars and 0.35 m, 0.5 m, 1.0 m and 2.0 m vertical poles of the disc-buckle type formwork support. In order to study the structural stability bearing capacity of the disc-buckle type formwork support, the experimental design was carried out according to the factors that should be considered in the actual project that affect the structural stability bearing capacity, the main influencing factors that should be considered were the lift height, and the working conditions. Working conditions include the working conditions of the central pole, the side pole and the corner pole. The lift height includes 0.5 m, 1.0 m and 1.5 m. The grouping of experimental design includes six experiments, Experiment 1: Working condition was set to central pole, lift height was set to 1.5 m. Experiment 2: Working condition was set to central pole, lift height was set to 0.5 m & 1.0 m. Experiment 3: Working condition was set to side pole, lift height was set to 0.5 m & 1.0 m. Experiment 4: Working condition was set to side pole, lift height was set to 0.5 m, 0.5 m & 0.5 m. Experiment 5 and Experiment 6: Working condition was set to corner pole, lift height setting was the same as the experiment 3 and experiment 4. The experiment loading method and the finite element model establishment method were available to view my published papers²⁷.

Finite element numerical analysis and verification

Euler equation $P_{cr} = \pi^2 EI_{min} / l^2$ was derived from the approximate differential equation $d^2w / dx^2 = M / EI$ of bending deformation. The critical stress equation $\sigma_{cr} = \frac{P_{cr}}{A} = \frac{\pi^2 EI}{(\mu l)^2 A} = \frac{\pi^2 E}{(\mu l / i)^2} = \frac{\pi^2 E}{\lambda^2}$ can be obtained from the critical load equation $P_{cr} = \pi^2 EI_{min} / (\mu l)^2$ of slender compressive bars with other end constraints, Material obeying Hooke's Law was the basis of the above differential equation. So only when the critical stress was less than the proportional limit σ_p , the Euler equation was correct, let σ_{cr} be less than σ_p , get inequality $\pi^2 E / \lambda^2 \leq \sigma_p$ or $\lambda \geq \pi \sqrt{E / \sigma_p}$.

It can be seen that the Euler equation was correct only when the flexibility λ of the compressive bar was greater than or equal to the limit value $\pi \sqrt{E / \sigma_p}$. λ_p represented this limit value, namely $\lambda_p = \pi \sqrt{E / \sigma_p}$, and the condition can be written as $\lambda \geq \lambda_p$. λ_p was related to the properties of the material. Different materials led to different values of λ_p . According to the research content of this paper, the material of the vertical pole was set to Q345A, and the proportional limit should be less than 345 MPa. If calculated according to 345 MPa, there was,

$$\lambda_p = \pi \sqrt{E / \sigma_p} = \pi \sqrt{206 \times 10^9 \text{ Pa} / 345 \times 10^6 \text{ Pa}} \approx 77$$

According to the length design of vertical pole in the experiment, the slenderness ratio $\lambda = \mu l / i = 140.83 \text{ cm} / 1.59 \text{ cm} \approx 89$ can be obtained, that was $\lambda = 89 > \lambda_p = 77$, so it was known that the stability calculation of the support formwork meets the applicable conditions of the Euler equation.

The stability calculation equation of compression bar was, $P / \varphi A \leq f$, so the critical load was $P_{cr} = \varphi \cdot f_y A$.

Among them, φ was represented stability coefficient, f_y was represented steel strength, A was represented cross-sectional area.

The results of the comparison analysis between the experimental and the finite element were shown in Table 3. Through the mutual verification of the above experiment and finite element, the correctness of the experimental results of the stability bearing capacity can be verified, the accuracy of the joint bending experimental was verified by the accuracy of the overall experimental results.

Conclusions

In this paper, the bending behavior of the disc-buckle type connection joints was studied by experiments, the failure mode, stress distribution and bending behavior of the connection joints of the disc-buckle formwork support were systematically studied, and it was verified that the connection characteristics of the connection joints of the disc-buckle formwork support were semi-rigid connections. The correctness of the finite element model was verified by comparing the experiment with the finite element analysis. Based on the accurate finite element model of the joints, the parametric analysis of the factors affecting the bending behavior of the joints was carried out. The recommended values of material strength and size thickness of components were proposed, and the maximum influencing factors of bending behavior of joints were obtained. The overall high formwork support system model was established based on the bending behavior of the semi-rigid connection joints, and the influencing factors of the high formwork support system were analyzed by finite element parametric analysis, the results of the experimental and finite element analysis was shown that:

The insertion depth affected by the mutual embedding of the wedge and the bolt hole on the disk-plate had an influence on the negative joint bending capacity, the drop depth of the wedge should not exceed 6 mm when locking. This also shown that the depth was not the greater the better, to control in a relatively reasonable range was more reasonable, for the construction workers of the construction operation made valuable comments. The initial position of the wedge insertion the disk-plate had no influence on the bending capacity. The thickness of the wedge was proportional to the joint bending capacity, and the optimal thickness of the wedge was 7 mm. The material constitutive of the wedge and the thickness of disk-plate had obvious influence on the bending capacity of joints. The optimal thickness of disk-plate was 10 mm and the optimal yield strength was between 450 and 500 MPa. The thickness of the disk-plate had an enhanced influence on the insertion depth of the wedge and the bending capacity of the material constitutive of the wedge. The results of the above analysis suggested the recommended values of material strength and size thickness for components, which provided valuable advice for the manufacturing process of components.

Data availability

All data generated or analysed during this study are included in this published article.

Received: 4 March 2024; Accepted: 6 January 2025

Published online: 13 January 2025

References

1. Cai, X. F., Zhuang, J. P. & Zhou, J. Z. Experimental research on torsional performance of right-angle coupled steel pipe joints. *Eng. Mech.* **29**(2), 107–113 (2012).
2. Lu, Z. R. et al. Experimental and theoretical study of the bearing capacity of fastener steel tube full-hall formwork support system. *China Civ. Eng. J.* **45**(1), 49–60 (2012).
3. Weesner, L. B. & Jones, H. L. Experimental and analytical capacity of frame scaffolding. *Eng. Struct.* **23**(6), 592–599 (2001).
4. Chan, S. L. & Cho, S. H. Second-order analysis and design of angle trusses Part I: Elastic analysis and design. *Eng. Struct.* **30**(3), 616–625 (2008).
5. Cho, S. H. & Chan, S. L. Second-order analysis and design of angle trusses, Part II: Plastic analysis and design. *Eng. Struct.* **30**(3), 626–631 (2008).
6. Sevim, B., Bekiroglu, S. & Arslan, G. Experimental evaluation of tie bar effects on structural behavior of suspended scaffolding systems. *Adv. Steel Constr.* **13**(1), 62–77 (2017).
7. Liu, H. B., Zhou, Y., Chen, Z. H. & Liu, Q. Structural performance and design method of new mortise-tenon full steel-tube scaffold. *Adv. Steel Constr.* **14**(2), 291–307 (2018).
8. Hadipriono Fabian, C. & Wang, H. K. Analysis of causes of falsework failures in concrete structures. *J. Constr. Eng. Manag.* **112**(1), 112–121 (1986).
9. Chen, Z. H. & Zhao, Z. W. Analysis of door-type modular steel scaffolds based on a novel numerical method. *Adv. Steel Constr.* **12**(3), 316–327 (2016).
10. El-Sheikh, A. Effect of member length imperfections on triple-layer space trusses. *Eng. Struct.* **19**(7), 540–550 (1997).
11. Li, G. Q. & Liu, Y. S. A nonlinear beam element considering initial imperfection. *Chin. J. Comput. Mech.* **22**(1), 69–72 (2005).
12. Chan, S. L. & Cho, S. H. Second-order P-Δ-δ analysis and design of angle trusses allowing for imperfections and semi-rigid connections. *Adv. Steel Constr.* **1**(1), 169–183 (2005).
13. Zhao, Z. W., Liu, H. Q., Dong, J. F. & Bian, Y. X. Buckling capacity of socket-template scaffold system without X-bracing. *J. Perform. Constr. Facil.* **34**(1), 1–14 (2020).
14. Zhao, Z. W., Liu, H. Q., Liang, B. & Yan, R. Z. Influence of random geometrical imperfection on the stability of single-layer reticulated domes with semi-rigid connection. *Adv. Steel Constr.* **15**(1), 93–99 (2019).
15. Abdel-Jaber, M., Beale, R. G., Shatarat, N. K. & Shehadeh, M. A. Experimental and theoretical investigations of spigot connections under cyclic loading. *Adv. Steel Constr.* **15**(1), 37–46 (2019).
16. Peng, J. L., Wang, S. H., Wang, C. S. & Yang, J. P. Stability study on scaffolds with inclined surfaces and extended jack bases in construction. *Adv. Steel Constr.* **17**(1), 73–83 (2021).
17. Ozyurt, E. & Wang, Y. C. A numerical investigation of static resistance of welded planar steel tubular joints under in-plane and out-of-plane bending at elevated temperatures. *Eng. Struct.* **199**(C), 109622 (2019).
18. Chen, Z. H. et al. Experimental and theoretical research on capacity of unbraced steel tubular formwork support based on sway frame with semi-rigid connection theory. *J. Build. Struct.* **31**(12), 56–63 (2010).
19. Zhang, H., Chandrangsu, T. & Rasmussen, K. J. R. Probabilistic study of the strength of steel scaffold systems. *Struct. Saf.* **32**(6), 393–401 (2010).
20. Xiao, M. K., Xu, C., Duan, J. & Tan, J. L. Research on the semi-rigid joint of disk lock steel tubular type for support system. *Sci. Technol. Eng.* **17**(12), 228–233 (2017).
21. Yuan, X. X. et al. A study on the stability bearing capacity of fastener-style tubular steel formwork-supports. *China Civ. Eng. J.* **39**(5), 43–50 (2006).
22. Lu, Z. R. et al. Study of the bearing capacity of fastener steel tube full hall formwork support using the theory of stability of pressed pole with three-point rotation restraint. *China Civil Eng. J.* **45**(5), 104–113 (2012).
23. Lu, Z. R. et al. Study on bearing capacity of fastener steel tube full hall formwork support system under eccentric load. *J. Dalian Univ. Technol.* **56**(1), 20–27 (2016).

24. Zhuang, J. P., Cai, X. F., Zheng, Y. Q. & Zhou, J. Z. Study on the overall stability of high and large formwork support system with fastening style steel pipe. *China Civ. Eng. J.* **49**(10), 57–63+87 (2016).
25. Yu, W. K., Chung, K. F. & Chan, S. L. Structural instability of multi-storey door-type modular steel scaffolds. *Eng. Struct.* **26**(7), 867–881 (2004).
26. Chu, A. Y. T., Chan, S. L. & Chung, K. F. Stability of modular steel scaffolding systems—Theory and verification. *Adv. Build. Technol.* **1**, 621–628 (2002).
27. Dong, J. F. et al. Experimental research and finite element analysis on structural stability of disc-buckle type formwork support. *Int. J. Steel Struct.* **22**(03), 748–766 (2022).
28. Metallic materials—Tensile testing—Part 1: Method of test at room temperature: GB/T 228.1–2010 (China Standards Press, 2010).
29. Dong, J. F. et al. Effective length correction factor of disc-buckle type scaffolding by considering joint bending stiffness and geometrical size. *PLoS ONE* **17**(10), e0276340 (2022).

Author contributions

J.D. was responsible for the numerical simulations and main manuscript text, Z.L. was responsible for experimental analysis, H.L. was responsible for the original research concept, Z.Z. as a corresponding author was responsible for part of the finite element analysis. M.L. and Z.C. analyzed the results. L.W. and X.G. was responsible for data interpretation. All authors reviewed the manuscript.

Funding

The Funding was provided by the National Natural Science Foundation of China (grant number 51974146) and Key R & D projects in Liaoning Province [Grant Number 2018Z30008] and Local Service Project of Liaoning Provincial Department of Education [Grant Number LJ2020FWL003].

Declarations

Competing interests

The authors declare no competing interests.

Ethical approval

This article does not contain any studies with human participants performed by any of the authors.

Informed consent

Informed consent was obtained from all individual participants included in the study.

Additional information

Correspondence and requests for materials should be addressed to J.D.

Reprints and permissions information is available at www.nature.com/reprints.

Publisher's note Springer Nature remains neutral with regard to jurisdictional claims in published maps and institutional affiliations.

Open Access This article is licensed under a Creative Commons Attribution-NonCommercial-NoDerivatives 4.0 International License, which permits any non-commercial use, sharing, distribution and reproduction in any medium or format, as long as you give appropriate credit to the original author(s) and the source, provide a link to the Creative Commons licence, and indicate if you modified the licensed material. You do not have permission under this licence to share adapted material derived from this article or parts of it. The images or other third party material in this article are included in the article's Creative Commons licence, unless indicated otherwise in a credit line to the material. If material is not included in the article's Creative Commons licence and your intended use is not permitted by statutory regulation or exceeds the permitted use, you will need to obtain permission directly from the copyright holder. To view a copy of this licence, visit <http://creativecommons.org/licenses/by-nc-nd/4.0/>.

© The Author(s) 2025